Electronic Supplementary Material (ESI) for Inorganic Chemistry Frontiers.

ELECTRONIC SUPPORTING INFORMATION

A microporous Mg^{2+} MOF with high selectivity for CO_2 and cation exchange property in a single-crystal-to-single-crystal fashion

Eleutheria Papazoi,[a] Antigoni Douvali,[a] Sofia Rapti,[a] Euaggelia Skliri,[b] Gerasimos S. Armatas,[b] Giannis S. Papaefstathiou,[c c] Xin Wang,[d] Zhen-Feng Huang,[d] Spyridon Kaziannis,[e] Constantine Kosmidis,[e] A. Hatzidimitriou,[f] Theodore Lazarides*[f] and Manolis J. Manos*[a]

[a.] *Department of Chemistry, University of Ioannina, 45110, Ioannina, Greece*
[b.] *Department of Materials Science and Technology, University of Crete 71003 Heraklion, Greece.*
[c.] *Laboratory of Inorganic Chemistry, Department of Chemistry, National and Kapodistrian University of Athens, Panepistimiopolis, Zografou 157 71, Greece.*
[d.] *School of Chemical and Biomedical Engineering, Nanyang Technological University, 62 Nanyang Drive, Singapore 637459, Singapore*
[e.] *Department of Physics, University of Ioannina, 45110, Ioannina, Greece*
[f.] *Department of Chemistry, Aristotle University of Thessaloniki, 54124 Thessaloniki, Greece.*

EXPERIMENTAL SECTION

Materials. All reagents and solvents were commercially available and used as received.

Synthesis of AEMOF-7. $Mg(NO_3)_2 \cdot 6H_2O$ (0.282 g, 1.1 mmol) was added as a solid into a stirred solution of NH_2H_2BDC (0.216 g, 1.2 mmol) in 5 mL DMAc/H_2O (9:1 *v/v*), in a Teflon cup. The mixture was stirred for ~ 5 min and then, the Teflon cup was transferred into a 23 mL Teflon-lined stainless steel autoclave. The autoclave was sealed and placed in an oven operated at 120 ˚C, remained undisturbed at this temperature for 20 h and then was allowed to cool at room temperature. The needle like crystals of **AEMOF-7** were isolated by filtration and dried in the air. Yield: 0.1 g.

Synthesis of AEMOF-7-Cu

A typical SCSC ion-exchange experiment of **AEMOF-7** with Cu^{2+} is the following:

A few crystals of **AEMOF-7** (5-10 mg) are immersed in a DMF solution of $Cu(NO_3)_2 \cdot 2.5H_2O$ (0.2 M) and remained undisturbed for 3-4 days. Then, the crystals of **AEMOF-7-Cu** were isolated by filtration, washed with DMF and diethylether and dried in the air. Single crystal X-ray analysis was conducted on a well-diffracting crystal of **AEMOF-7-Cu**. Note that several crystals of the exchanged material were tested and found to have identical unit cell parameters.

For the experiments with polycrystalline samples, finely ground crystals of the MOF (~10 mg) were treated with dilute Cu^{2+} DMF solutions (MOF:Cu molar ratio was 0.4) for one day. The exchanged sample was then isolated via filtration, washed with DMF and diethylether and dried under vacuum. The content of Cu in the exchanged material was measured via anodic stripping voltammetry.

Synthesis of Ni^{2+} and Co^{2+}-exchanged compounds

The isolation of Ni^{2+} and Co^{2+}-exchanged materials has been done by reacting polycrystalline **AEMOF-7** and dilute DMF solutions of Ni^{2+} and Co^{2+} salts respectively. The MOF:Ni or Co molar ratio was 1:0.4. The content of Ni or Co in the exchanged materials was determined via anodic stripping voltammetry.

Physical measurements.

PXRD, TGA, IR. PXRD diffraction patterns were recorded on a Bruker D8 Advance X-ray diffractometer (CuKa radiation, λ = 1.5418 Å). IR spectra were recorded on KBr pellets in the 4000-400 cm^{-1} range using a Perkin-Elmer Spectrum GX spectrometer. Thermogravimetric analysis (TGA) was carried out with a Shimatzu TGA 50. Samples (10±0.5 mg) were placed in quartz crucible. Samples were heated from ambient temperature to 600 ^oC in a 20 mL/min flow of N_2. Heating rate of 10 ^oC/min was used.

Solid state UV-Vis spectroscopy. Solid state UV/Vis spectra were obtained on a Shimadzu 1200 PC in the wavelength range of 200-800 nm. $BaSO_4$ powder was used as a reference (100% reflectance) and base material on which the powder sample was coated. The reflectance data were converted to absorption using the Kubelka-Munk function.

Gas sorption measurements. Nitrogen adsorption and desorption isotherms were measured at liqud nitrogen temperature (–196 ^oC) on a Quantachrome NOVA 3200*e* sorption analyzer. CO_2 and CH_4 adsorption experiments at –10 ^oC and 0 ^oC were performed using a Hiden IGA-003 gravimetric sorption analyzer. Before analysis, the samples were EtOH-exchanged, activated via supercritical CO_2 drying and degassed at 80 ^oC under vacuum (<10^{-4} mbar) for 12 h. The specific

surface area was calculated using the Brunauer-Emmet-Teller (BET) method (Ref.:S. Brunauer, L. S. Deming, W. E. Deming and E. Teller, *J. Am. Chem. Soc.*, 1940, **62**, 1723-1732) on the CO_2 adsorption data at 0 ^oC in the relative pressure (P/P_o) range of 0.017–0.026. In general, the use of CO_2 as an adsorptive is considered as a reliable approach to determine the surface area, especially of microporous solids [F. Rouquerol, J. Rouquerol, K. Sing, Adsorption by Powders and Porous Solids: Principles, Methodology and Applications, Academic Press, London, 1999, Chap. 6 and Chap. 9]. In particular, for porous solids containing ultramicropores (pore size < 7 Å) such as the compound presented in this work, the diffusion of N_2 molecules at 77 K into micropores is very slow. This may result in a N_2 adsorption analysis under non-equilibrium conditions, giving erroneous results of the measurement. These limitations can be overcome by using CO_2 adsorption at elevated temperature (e.g. 273 K), where CO_2 molecules can more easily access ultramicropores. Moreover, since the kinetic diameter of CO_2 (0.33 nm) is smaller than that of N_2 (0.36 nm), CO_2 molecules can permeate more easily through small micropores. The pore size distribution plot was determined from the CO_2 adsorption data at 0 ^oC using the density functional theory (DFT) method (assuming slit shape pores).

i. *Gas selectivity using the IAST approach*

Gas selectivity was predicted using the ideal adsorbed solution theory (IAST) (Ref.:A. L. Myers, *Adsorption*, 2003, **9,** 9-16) from the equations:

$$s_{i,j} = \frac{x_i/y_i}{x_j/y_j} = \frac{p_j^0}{p_i^0} \qquad (1)$$

$$p = \sum_{i}^{j} p_i^0 x_i$$

(2)

where, $s_{i,j}$ is the selectivity for the adsorbates i and j, $y_i(=1-y_j)$ and $x_i(=1-x_j)$ are the molar fractions of the component i in the gas phase and the adsorbed phase, respectively, p_i^0 and p_j^0 are the pure component pressures for i and j, respectively, and p the total pressure of the gas mixture.

A more detailed description of these gas selectivity calculations is given elsewhere (Ref.:G. S. Armatas and M. G. Kanatzidis, *Nat. Mater.*, 2009, **8**, 217-222).

ii. *Isosteric heat of adsorption*

The gas adsorption isotherms acquired at different temperatures (i.e., –10 ^{o}C and 0 ^{o}C) can be described and analyzed using a virial-type equation (Ref.:L. Czepirski and J. Jagiello, *Chem. Eng. Sci.*, 1989, **44**, 797-801):

$$\ln p = \ln v + \frac{1}{T}\sum_{i=0}^{m} a_i v_i + \sum_{i=0}^{m} b_i v^i \qquad (3)$$

where, p is the pressure (Torr), v is the adsorbed amount (mmol g^{-1}), T is the temperature (K), a_i and b_i are adjustable parameters, and m and n represent the order of polynomials required to adequately describe the isotherms.

The coverage-dependent isosteric heat of adsorption, Q_{st}, is then calculated by the following expression:

$$Q_{st} = -R\sum_{i=1}^{m} a_i v_i \qquad (4)$$

where, R is the universal gas constant.

Fluorescence spectra. The fluorescence spectra of **AEMOF-7** and **AEMOF-7-Cu** were measured on a Hitachi F7000 spectrofluorometer equipped with a powder sample holder. The light source was a Xenon arch lamp and the detector a red sensitive Hamamatsu R928 photomultiplyer tube. Appropriate long pass filters were used to remove scattering from the sample and the monochromators.

Anodic stripping voltammetry (ASV). The determination of Cu, Ni and Co was performed with anodic stripping voltammetry (ASV) using Trace Metal Analyzer (797 VA Computrace, Metrohm AG Ltd, Switzerland). The exchanged solid materials (~10 mg) were dissolved in water (~10 mL). After dilution of these solutions (100-1000 times), the analysis has been done following the AN-V-086 (Cu analysis) and AN-V-087 (Ni, Co analysis) protocols developed by Metrohm (http://www.metrohm.com/en/applications/#). This method is capable to determine Cu, Ni or Co in ppt levels (detection limits for these metal ions are as low as 0.05 ppb).

Proton conductivity measurements. Pellet of 14 mm in diameter and 0.16 mm thick was prepared by pressing material (about 40 mg) at 14-15 MPa. The proton conductivity of the sample was estimated tested by two-point probe alternating current (AC) impedance spectroscopy technique. The impedance was measured with a frequency response analyzer

(Autolab workstation) over a frequency range from 1 Hz to 10^5 Hz and 10 mV perturbation. The samples were covered with the two copper blocking electrodes in a measurement cell and placed under room temperature environment. Note the measurements were repeated three times to get reproducible results. Proton conductivity (σ) was calculated according to the relationship: $\sigma = l/AR$, where R is the sample resistance, A is the cross-section of the sample, and l is the length between the electrodes. The theoretical derivation from Nyquist plot to the ohmic resistance of the sample is according to $Z = R_s + 1/[(1/R) + j2\pi fC_{dl}]$, where R_s is solution resistance, f is the frequency and C_{dl} is the capacitance.

Single crystal X-ray crystallography. The single crystal X-ray diffraction measurements were carried out with a Bruker Apex-II CCD using graphite-monochromatized Mo Kα radiation. The data were collected at room temperature over a full sphere of reciprocal space. Cell refinement, data reduction and numerical absorption correction were carried out using Bruker SAINT software package (Bruker, *Apex2*, *Version 2*, Bruker AXS Inc., Madison, Wisconsin, USA, 2006). The intensities were extracted by the program XPREP (Sheldrick, G. M. In *SHELXTL*; 5.1 ed.; Bruker-AXS: Madison, WI, 1998). The structures were solved with direct methods using SHELXS and least square refinement were done against F_{obs}^2 using routines from SHELXTL software (Sheldrick, G. M. In *SHELXTL*; 5.1 ed.; Bruker-AXS: Madison, WI, 1998). For the structure of **AEMOF-7-Cu**, an occupational disorder model was used. This means that for each metal site we applied a model with mixed Mg and Cu atoms. Using EADP and EXYZ commands, both atoms were fixed at the same displacement parameters and atomic coordinates. Thus, we refine only the occupancies for each atom. Careful inspection of the solution shows no evidence of two overlaid positions.

CCDC 1519902 and 1519903 contain the supplementary crystallographic data for this paper. These data can be obtained free of charge via www.ccdc.cam.ac.uk/data_request/cif.

Time resolved fluorescence measurements. The time-resolved fluorescence experiments were performed in the Central Laser Facility of the University of Ioannina using a custom made setup, which is presented in Scheme S1.

The setup incorporates a Ti:Sapph fs laser system producing irradiation at a central wavelength of 800n with ~67nm FWHM bandwidth, corresponding to a laser pulse of ultrafast duration ~25f, and a maximum energy per pulse of 5.5mJ at 1KHz repetition rate. The 800nm laser beam is frequency doubled in a KDP second harmonic generation crystal (type-I phase matching). Due to the large thickness of the KDP crystal (2.5cm) the phase matching process results in a second harmonic (SH) beam with a relatively narrow bandwidth ~0.36nm (a process referred to in the literature as spectral compression, Ref.: M. Marangoni, D. Brida, M. Quintavalle, G. Cirmi, F. M. Pigozzo, C. Manzoni, F. Baronio, A. D. Capobianco, e G. Cerullo, «Narrow-bandwidth picosecond pulses by spectral compression of femtosecond pulses in a second-order nonlinear crystal», Optics Express, vol 15, issue 14, page 8884–8891, 2007), corresponding to a Fourier transform limited pulse of ~600fs duration. The thick second harmonic generation (SHG) crystal approach offers enhanced conversion efficiency, while at the same time a strong broadening effect on the SH pulse duration, which reduces the irradiation intensity and, therefore, restricts the possibility of non-linear interactions or photo-induced degradation of the sample. Moreover, the central wavelength of the SH can be tuned by careful adjustment of the KDP crystal orientation with respect to the 800nm beam pointing and polarization axis (S-polarization right after the half wave plate $-\lambda/2-$) and the optimization of the compressor of the fs laser system. For the experimental data shown in the present work the SH beam was tuned at a central wavelength of

in the range of 374-378nm and its intensity on the sample surface is estimated to be ~(1-3)×10^6W/cm^2.

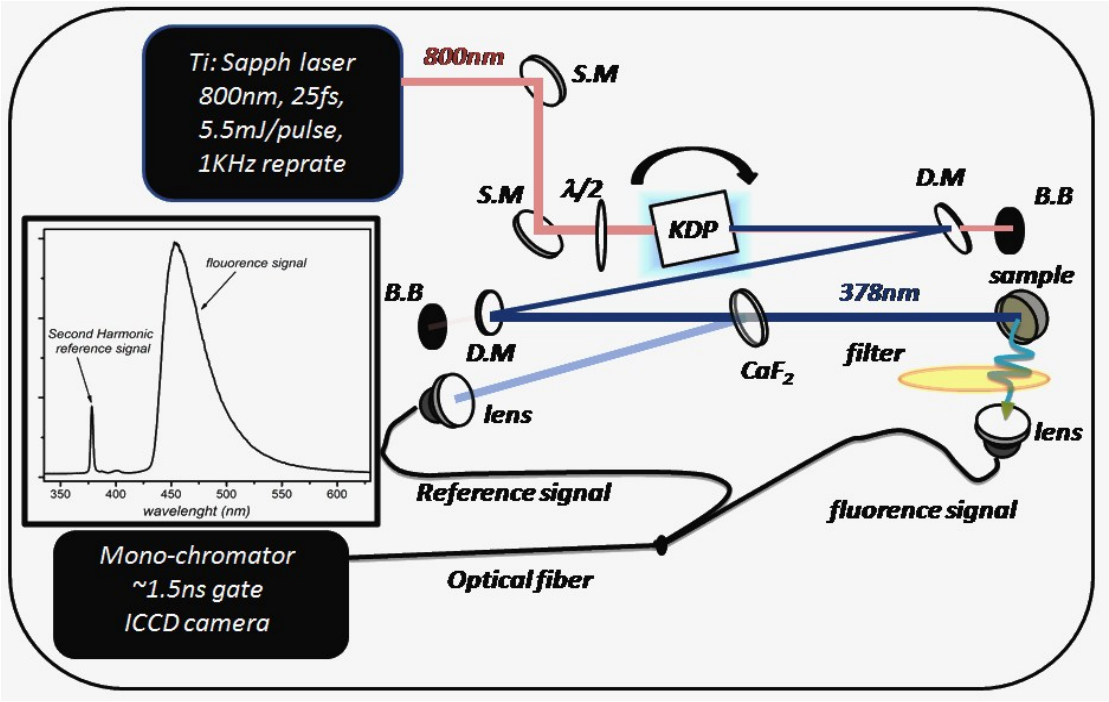

Scheme S1. Ti: Sapphire fs laser system, SM: silver mirrors, λ/2 half wave-plate at 800nm, KDP second harmonic generation crystal, D.M: dichroic mirrors– high reflectivity at the SH region, CaF_2 window, long pass filter (λ>430nm), two way oprical fiber bundle, Spectograph (monochromator – ICCD camera)

A couple of dichroic mirrors with high reflectivity >99% at the SH wavelength region are employed for isolating the SH beam from the fundamental one. Moreover, a CaF_2 window is used as a SH beam sampler, providing a reference signal for energy of the SH pump beam, while the fluorescence signal is acquired. The fluorescence and the SH reference signals are collected with a two way fiber bundle and the corresponding spectra are recorded using an Andor intensified gated i-CCD camera coupled to a Czerny – Turner monochromator. The i-CCD

detector specifications suggest that it should be feasible to record slices in time of the fluorescence signals as short as 1.5ns. However, the time resolved measurement resolution is poorer due to the time-jitter between the actual time of arrival of the SH beam on the sample and the TTL pre-trigger provided by the fs laser system, which is used for the synchronization of the i-CCD detector and the laser output. The response function of the home built spectrometer is recorded by integrating the signal of the SH reference beam, which is effectively instantaneous compared to the ns timescale, as a function of the TTL pre-trigger and the i-ICCD detector gate. The corresponding response function is shown in Fig.S12. The fluorescence dynamics data are fitted with a double exponential decay function taking into account that the data are convoluted with the time-response function, which is specified for each experimental run. Both the deconvolution and the fitting process have been tested on different molecular targets, which are typically used as test samples in time-resolved fluorescence spectroscopy (Ref: Standards for Nanosecond Fluorescence Decay Time Measurements. Anal Chem. Vol. 55, pages 68-73, 1983). During the time-resolved measurements, the monochromator and the i-CCD detector parameters are set for the highest photon recording efficiency, which compromises the wavelength spectra resolution to a value of ~1nm.

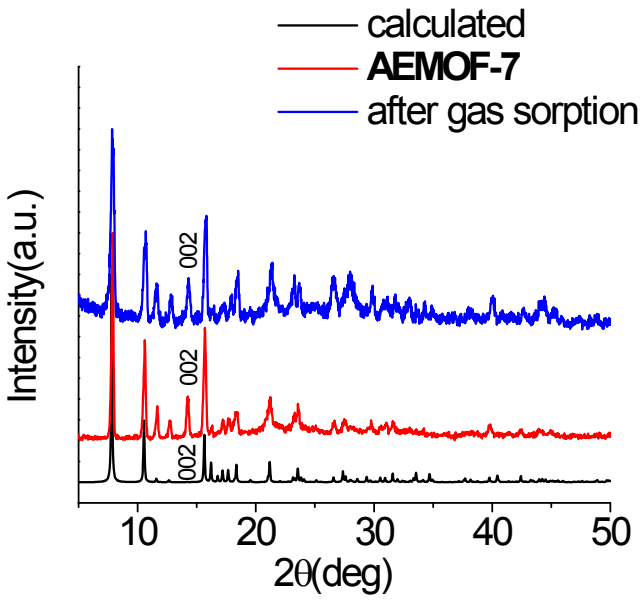

Fig. S1. Experimental and calculated (from single crystal X-ray data) PXRD patterns of **AEMOF-7** and PXRD pattern of the MOF after the gas sorption. The differentiation of some peak intensities between calculated and experimental patterns is due to strong preferred orientation effects due to the needle-like shape of the MOF crystals. For instance, due to strong preferred orientation the weak peak assigned to *002* reflection is appeared with relatively high intensity in the experimental PXRD patterns.

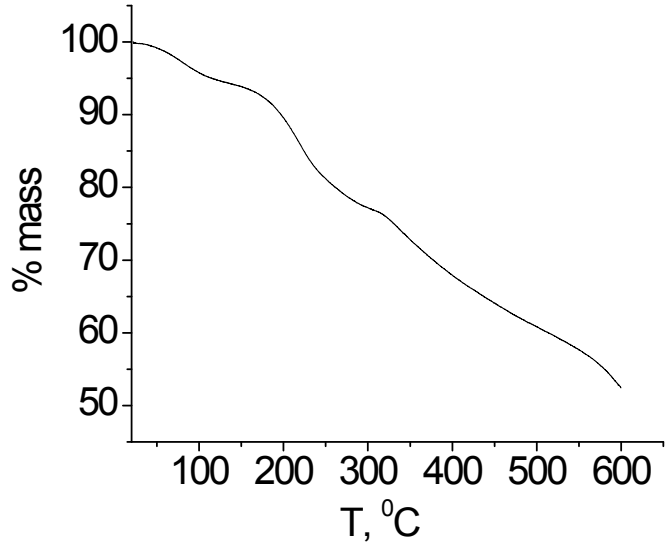

Fig. S2. The TGA data for **AEMOF-7** measured under N_2.

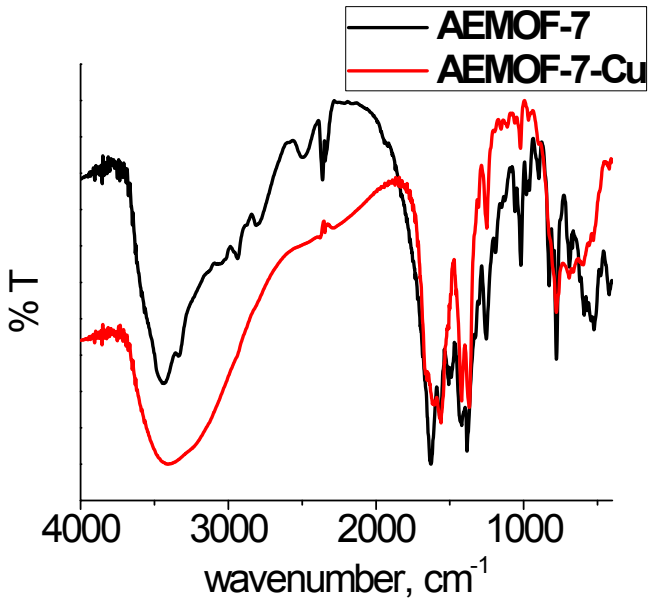

Fig. S3. The IR spectra of **AEMOF-7** and **AEMOF-7-Cu**.

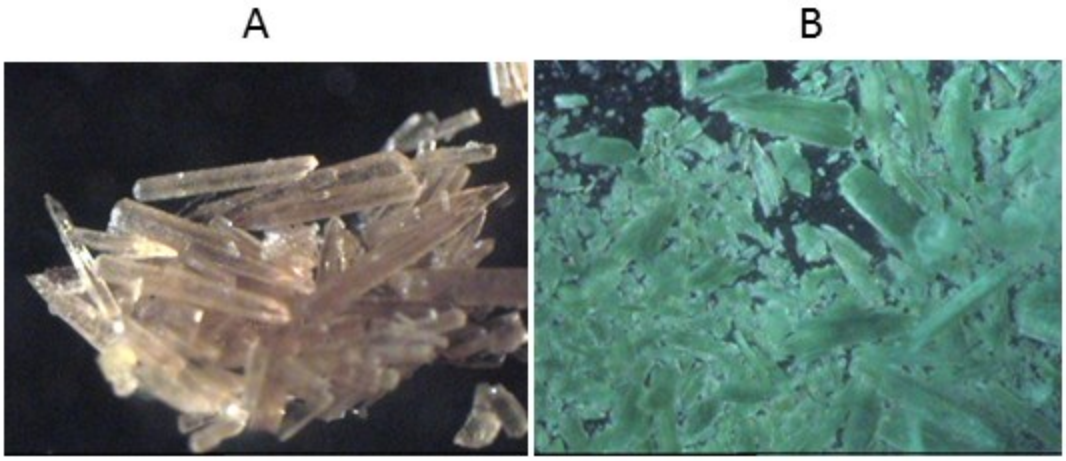

Fig. S4 . Images of crystals of **AEMOF-7** (A) and **AEMOF-7-Cu** (B).

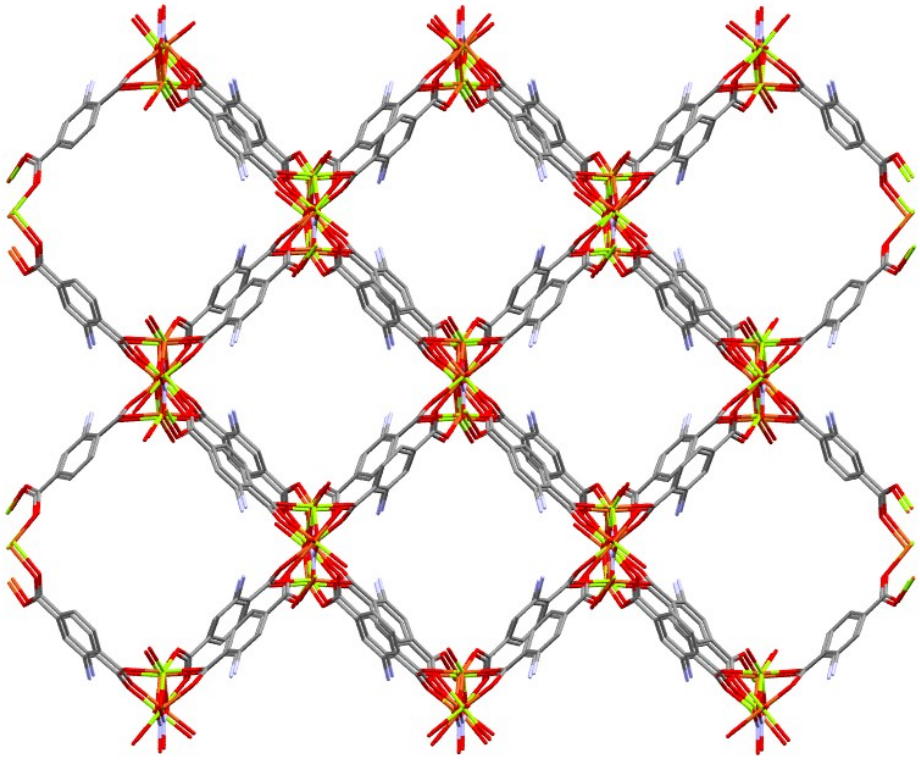

Fig. S5. Representation of the structure of **AEMOF-7-Cu** viewed down the a-axis. The H atoms and lattice solvent molecules were omitted for clarity. Color code: Mg/Cu, green; O, red; N, blue; C, grey.

Fig. S6. Photos of polycrystalline powder samples of **AEMOF-7** (left) and **AEMOF-7-Cu** (right).

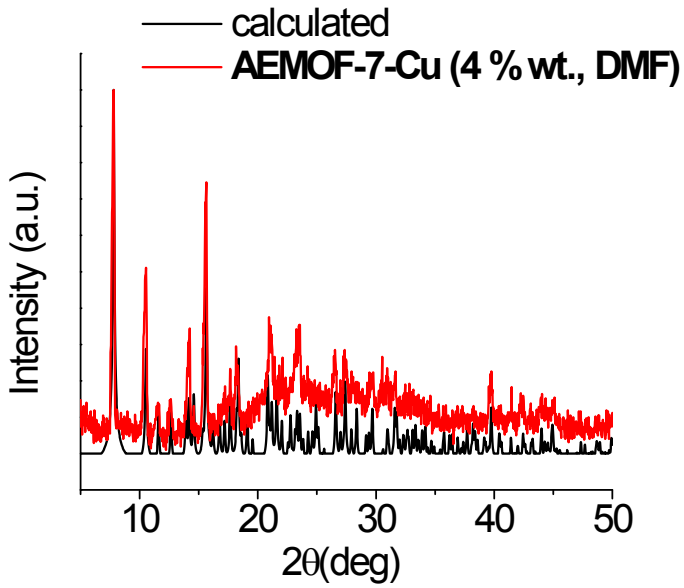

Fig. S7. Experimental (Cu^{2+} exchange reaction in DMF, Cu content of exchanged material = 4 % wt.) and calculated (from single crystal X-ray data) PXRD patterns of **AEMOF-7-Cu.**

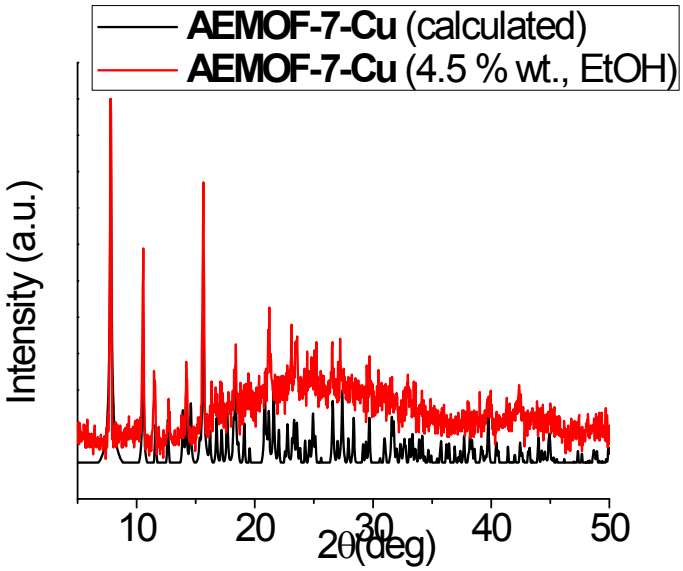

Fig. S8. Experimental (Cu^{2+} exchange reaction in EtOH, Cu content of exchanged material = 4.5 % wt.) and calculated (from single crystal X-ray data) PXRD patterns of **AEMOF-7-Cu.**

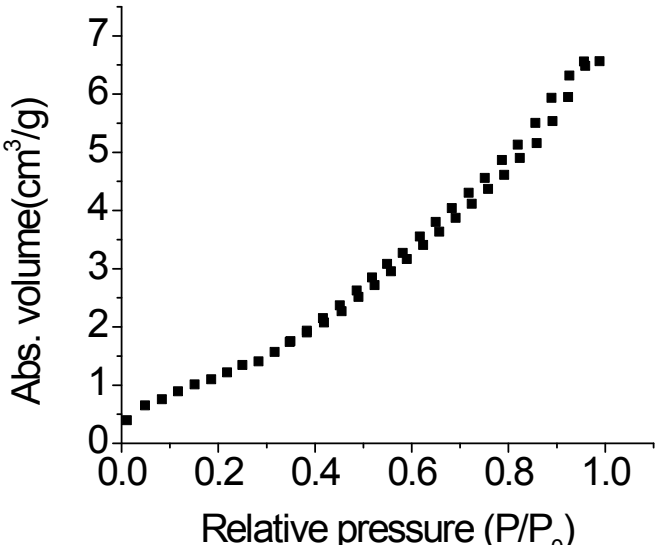

Fig. S9. N_2 adsorption isotherm at 77 K for **AEMOF-7.**

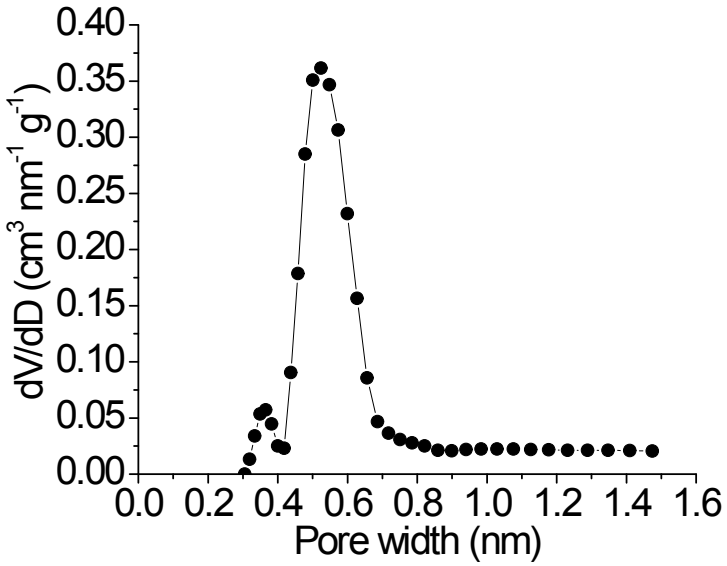

Fig. S10. The DFT pore size distribution for **AEMOF-7.**

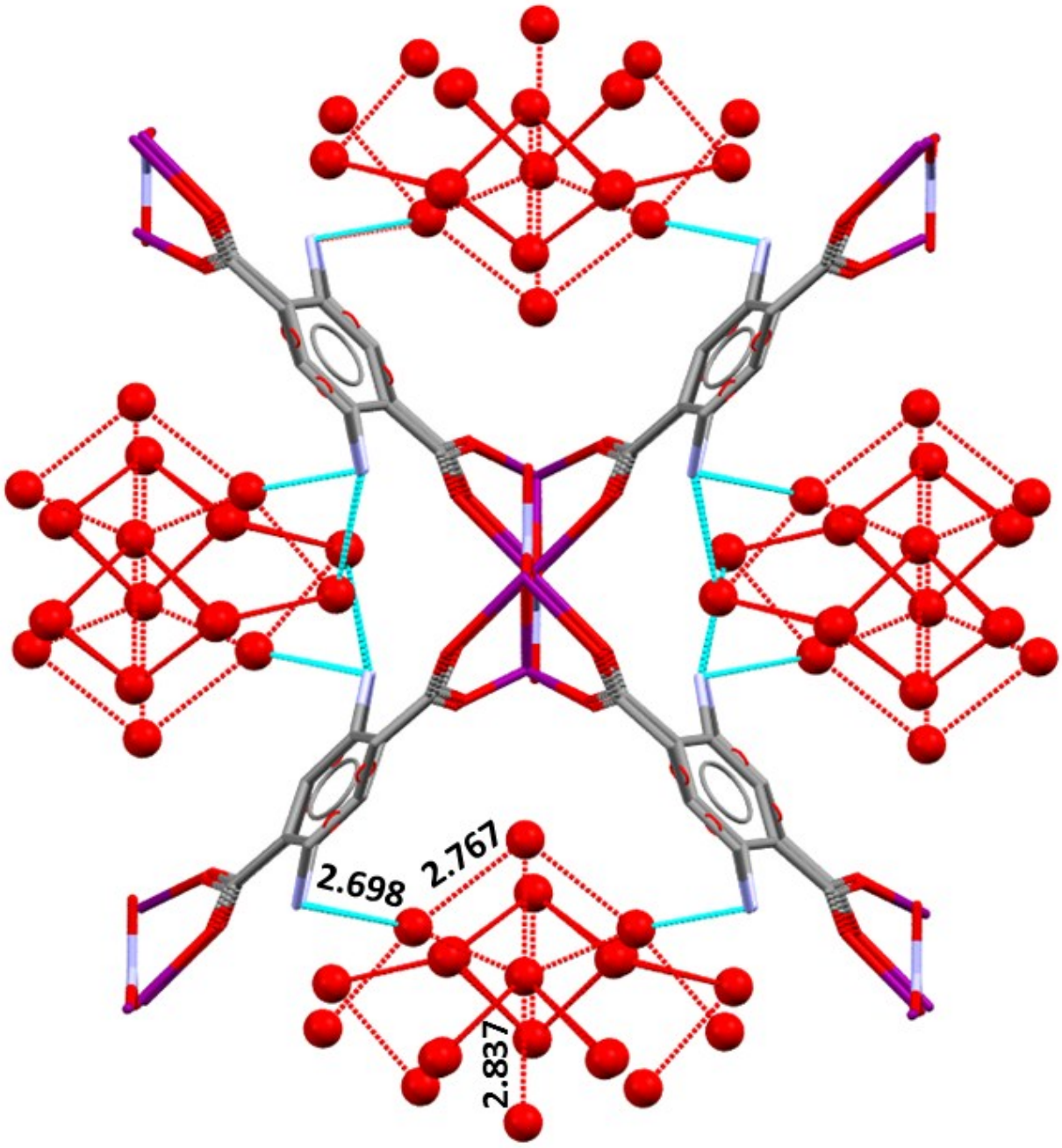

Fig. S11. The hydrogen bonds (red and cyan dashed lines) in which lattice water solvents (red balls) are involved in the structure of **AEMOF-7**. Selected H-bond distances are also indicated. Color code: Mg, purple; O, red; C, grey; N, blue.

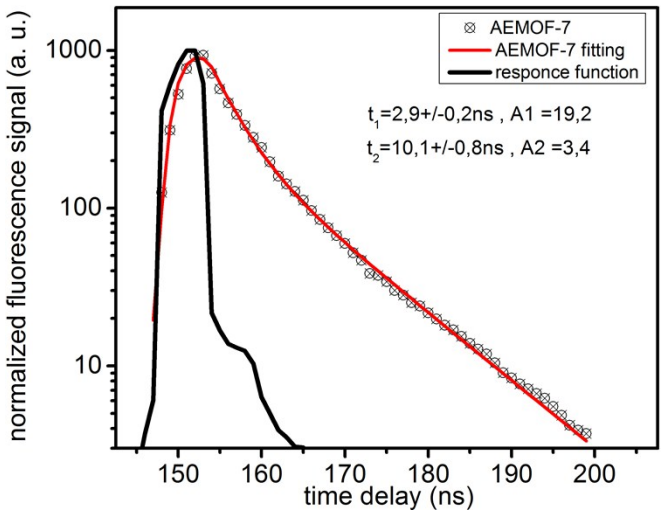

Fig. S12. Time resolved emission decay signals for **AEMOF-7**.

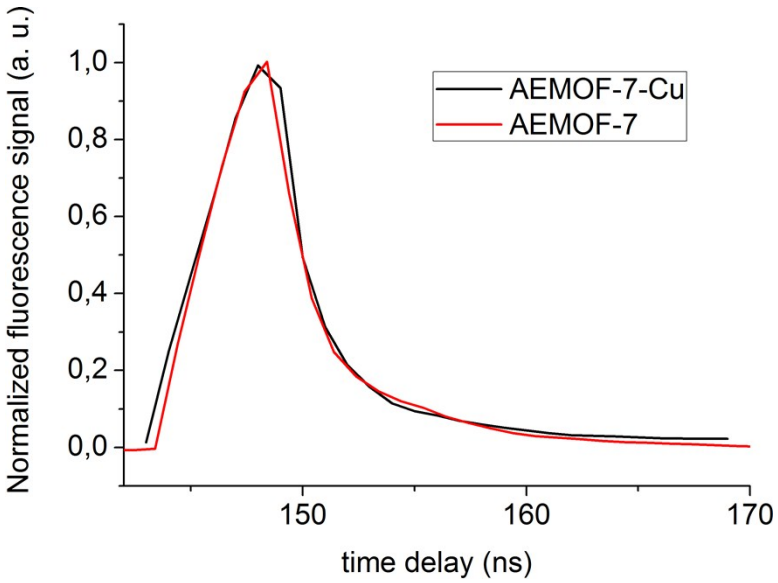

Fig S13. Comparison between the normalized time-resolved emission decay signals of **AEMOF-7** and **AEMOF-7-Cu**.